An Investigation of Mixing in Micro Coiled Flow Inverter in Varying Tube Diameter with Fixed Reynolds Number

JOANNE ZI EN SOH, EKO SUPRIYANTO
Faculty of Biosciences and Medical Engineering Department
Universiti Teknologi Malaysia
81300 Johor Bahru, Johor
MALAYSIA
joanne.sohze@gmail.com eko@utm.my

Abstract: - Micro-scaled Coiled Flow Inverter (MCFI) is a scaled down version of a Coiled Flow Inverter (CFI) which utilizes the principle of flow inversion for process intensification. MCFI is constructed with tubing less than 1.0mm. The microfluidic nature of MCFI caused by low Reynolds number (Re) laminar flow posed as a challenge to achieve effective mixing. Simulation was implemented with Computational Fluid Dynamics (CFD) software FLUENT to visualize the mixing of MCFI with different diameters. Fluid flow of the mixing of two water bodies was simulated. Geometry of the MCFI was designed with tubing diameters of 1.0mm, 0.8mm, 0.6mm and 0.5mm to investigate the effect of cross-sectional diameter towards mixing efficiency. The curvature ratio (λ) was fixed at 10 to reduce the complexity of the system. Fluid flow rate was calculated and adjusted to obtain Re 250 for each tubing size. Velocity profile of tubing within the range of diameter investigated showed negligible difference. Simulation results showed a parabolic velocity profile for straight tube, while skewed velocity profiles were observed within the straight coil and MCFI. MCFI with the tubing diameter of 0.5 mm achieved complete mixing at normalized tube length of 0.69, equivalent to 175mm. MCFI with ID 1.0 mm showed 54.5% mixing, while MCFI with ID 0.8 mm and 0.6 mm showed 69.6% and 78.9% mixing respectively at the outlet. Similarly, fluid in straight tube and straight coil had also failed to achieve complete mixing. Results obtained suggested smaller tubing diameter indeed led to better mixing process in MCFI, in expense of an increase in pressure.

Key-Words: - Computational Fluid Dynamics (CFD), Coiled Flow Inverter (CFI), Micro-Coiled Flow Inverter (MCFI), Reynolds number, Laminar Flow, Diffusive Mixing

1 Introduction

Mixing within a microfluidic domain generally depends on molecular diffusion to achieve a uniform spatial distribution in solute concentrations. Fluid flow in domain with low Reynolds number results in laminar flow, in which fluid flows in parallel layers without turbulence. Coiled configuration, namely helical mixing element, introduced secondary flow within a laminar flow domain by enforcing a centrifugal force acting outwards to the outer wall of a curvature. However, there exists a region in which fluid mixing progress slowly regardless of prolongation of tubing length, due to the presence of a laminar region unaffected by the centrifugal force [1]. Coiled Flow Inverter, as an extension of the helical mixing element, is constructed based on the principle of complete flow inversion. Constructed with coiled tube geometry with 90 degree bends at equal intervals of length, CFI was designed to induce Dean Vortices rotating corresponding to the 90 bending [4].

Various studies performed through numerical and experimental methods had proven that the CFI configuration improved mixing [2], [6], and thermal distribution [3], [5]. In the process industry, computer simulations proved CFI to be beneficial in liquid-liquid mixing. An evaluation of cross-sectional velocity profile and scalar concentration of liquid flow concluded significant increment in mixing as compared to a straight tube and helical mixing element of equal tube length [5]. Experimental works confirmed the enhanced mixing of CFI in which fluids achieve a narrow residence time distribution even under laminar flow [9]. CFI has found application numerically in polystyrene synthesis [7], and experimentally as a reactor for production of biodiesel by the transesterification of fatty acids [10].

CFI has recently been scaled down to micro-dimensions for process intensification [8], specifically as a micro heat exchanger. Micro-coiled flow inverter (MCFI) is constructed from tubing with diameter of equal or less than 1 mm. Results

showed that MCFI possessed higher thermal merit of up to 4-fold improvement compared to straight tube with equivalent cross sectional area, and almost 40% improvement compared to micro-hellical coil. A study on residence time distribution curves from different MCFI reactor setups concluded that the shape of the reactor had negligible effect on the axial dispersion [9], demonstrating the versatility of the design of MCFI based on the space restrictions and applications. MCFI has been applied in a liquid-liquid extraction system[10], [13], used in addition to the generation of slug flow in an n-butyl acetate/acetone/water test system, enhancing efficiency of up to 20% in comparison to straight capillaries.

2 Materials and Method

As the reduction in tubing diameter led to an increase in pressure drop, it is of interest to determine the largest diameter allowable to still achieve efficient mixing. In the present work, a computational fluid dynamics (CFD) study was performed in tubing with circular cross-section of different tube diameter constructed into a MCFI to understand the effect of tube diameter towards the mixing of two miscible fluids under laminar flow with same Re value

2.1 Software

CFD simulation was carried out with the software FLUENT in ANSYS 15. In this study, a liquid-liquid flow system of water-based dyes, here on considered 'red dye' and 'blue dye', was injected into the MCFI, and left to interact. The fluid properties of the water soluble dyes were assumed insignificant due to dilution. Thus, the simulation was carried out with the properties of liquid water including density and dynamic viscosity.

2.2 Governing Equations

To solve the conservation equations for chemical species, species transport model was used for simulation purposes. This model predicts the local mass fraction of each species by solving the convection-diffusion equation for the ith species, which is as below.

2.2.1 Conservation Equation

$$\frac{\partial}{\partial t}(\rho Y_i) + \nabla \cdot (\rho \vec{v} Y_i) = -\nabla \cdot \vec{J}_i + R_i + S_i \quad (1)$$

where the letters ρ ,*Y*, $\vec{v}$, $\vec{J}$, *R* and *S* indicates the density, local species mass fraction, velocity vector, species diffusion flux, the net rate of production of species I and the rate of creation by addition from the dispersed phase. Each species is denoted by the suffix *i*.

2.2.2 Diffusion Flux

In this study, due to the non-reactive nature of the mixing of dyes, species transport was steered by mass diffusion caused by the diffusion flux, $\vec{J}$. This is dependent on the concentration and temperature gradient. Ficks Law, i.e. the dilute approximation method was used to describe the scalar transport.

$$\vec{J}_i = -\rho D_{i,m} \nabla Y_i - D_{T,i} \frac{\nabla T}{T} \quad (2)$$

where Di,m is the mass diffusion coefficient for species I in the mixture and DT,i is the thermal diffusion coefficient.

2.3 Physical Geometry

Three MCFI geometries were constructed consisting of four straight coils connected with 90 degree bends in between, forming 4 arms of the MCFI. The inner tubing diameter (ID) was varied from 1.0mm, 0.8mm, and 0.5mm. The curvature ratio (λ) is the ratio of loop diameter over tubing diameter. The loop diameter (Dc) for each MCFI was modified to a curvature ratio of 10 corresponding to the tubing diameter. Besides the variance in tubing diameter, other parameters such as pitch and curvature ratio of the MCFI were identical to avoid complexity during the evaluation of mixing.

In addition to MCFI, geometries of straight tube and straight coil with equivalent tube length used to construct the MCFI, as shown in Fig. 1, were also constructed to compare the mixing efficiency. Reynolds number of 250 was achieved in each individual MCFI through an adjustment of flow rate.

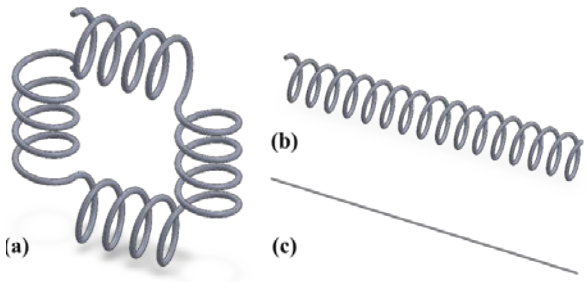

Fig. 1 Geometry design of (a) MCFI, (b) straight

coil, and (c) straight tube with equivalent tube diameter and length

2.4 Mesh Topology

A non-uniform, structured grid topology was generated for computations of model equations. Three different mesh sizes constructed from hexahedral cells were generated, by varying the number of cross sectional and axial cells incrementally, as shown in Fig. 2. This led to three sets of mesh with total cells of 929556, 1474666 and 2457948. Grid independence was checked for the pressure drop within the MCFI. Pressure drop in units of Pascal was calculated to be 1732, 1743 and 1743 accordingly, which meant that the mesh size of 147466 was sufficient to shorten calculation time without compromising accuracy.

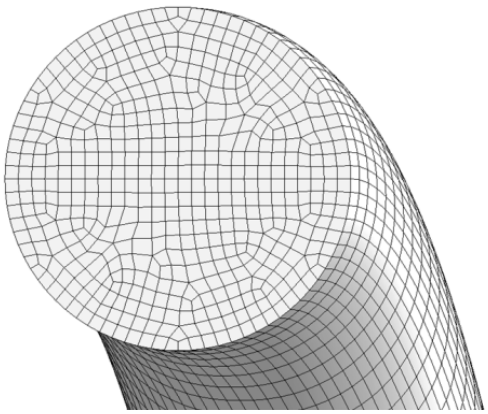

Fig. 2 Mesh topology at the inlet extended throughout the geometry

2.5 Mixing Efficiency

Mixing is considered ideal when a cell contained equal parts of both fluid bodies, in this case, the water-based dyes, resulting in a local mass fraction of value of 0.5. An evaluation of the tube cross-section regarding the percentage of cells with a value of 0.5 represented the percentage of fluid mixing

$$\%\, Mixing\,, \theta = {}^{N_{node=0.5}}/_{N_{cross\ section\ nodes}} \times 100\% \quad (3)$$

3 Results and Discussion

For validation, the velocity profile at different bends was generated with the proposed model and compared to the numerically computed results of published literature which focused on the process of heat transfer in MCFI. Fluid flow was simulated in MCFI ID of 0.5mm and λ of 10, similar to the geometry constructed for this study. Flow rate was adjusted to achieve Re of 434 as presented in literature.

Results of the horizontal and vertical centreline in Fig. 3 showed good agreement with the numerical prediction published in [6].

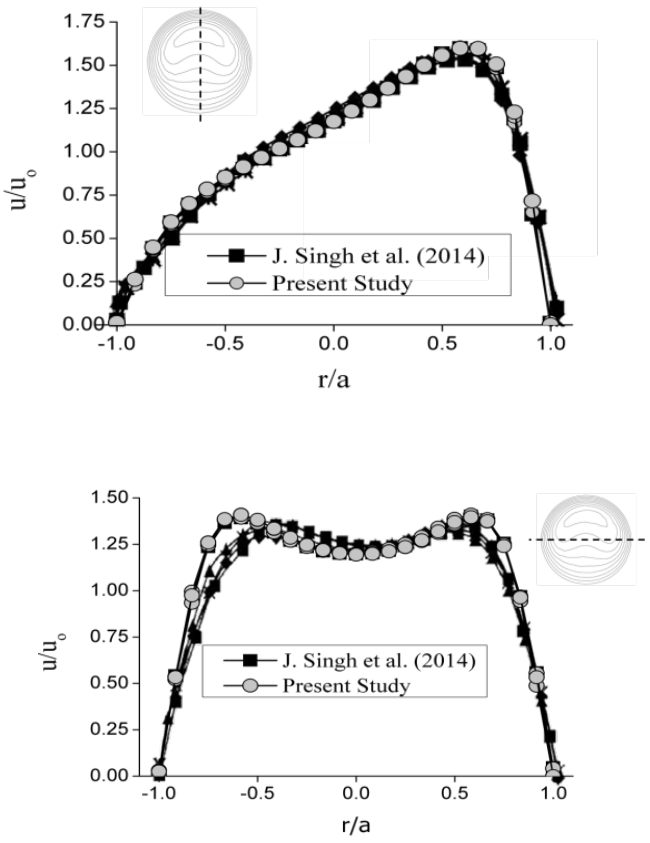

Fig. 3 Comparison of velocity profile in MCFI with data from literature for (top) vertical and (bottom) horizontal centreline

3.1 Pressure Drop

As the reduction in tube diameter brought along an increase in pressure drop across the MCFI, the pressure drop was plotted against tube diameter to highlight the relationship between the variables. According to Fig 4, tubing with 1.0mm diameter showed the lowest pressure drop with 621 Pa. The pressure drop increased in an almost exponential behaviour as the tube diameter was reduced gradually to 0.8mm, 0.6mm and 0.5mm with values of 9.79 kPa, 17.47 kPa and 24.95 kPa correspondingly.

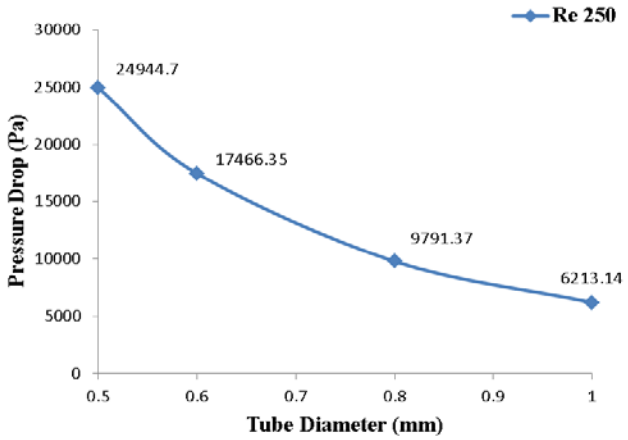

Fig 4. Pressure drop across tubing of 0.5≤ID≤1.0mm

3.2 Velocity Profile

Velocity profile for fluid flow within MCFI with tube diameter of 1.0mm, 0.8mm, 0.6mm and 0.5 mm is shown in Fig. 5. Fluid in coiled tubing and MCFI is subjected to a centrifugal force, causing the velocity profile to skew towards the outer wall. In response to the presence of 90˚ bending between each arm the velocity profile also rotated.

As a result the region of maximum velocity orientate in 4 different directions. This phenomenon is crucial for the manifestation of flow inversion, as fluid going through the bends was forced to realign with the different velocity profile orientations, mimicking turbulence in an otherwise laminar flow. Comparing MCFI with different tube diameter, the velocity profile showed negligible difference as the tubing diameter reduced from 1.0 mm to 0.5 mm.

The velocity profile for other tubing configuration is shown in Fig 6. For straight coil, the velocity profile skewed one-sided aligning to the outer wall due to the centrifugal force acting on the fluid within the coil. Fluid from the inner wall moved towards the outer wall, causing a collection of high velocity fluid at the region neighbouring the outer wall. This velocity profile was observed to extend throughout the entire length of the coil.

For straight tube, the velocity profile was parabolic with a maximum velocity at the middle of the tube. This resembled a typical laminar flow profile adhering to the 'no-slip boundary' condition, in which fluid adjacent to the wall was considered stationary with zero velocity. Moving inwards, fluids flowed in layers with increasing velocity to achieve a maximum velocity in the middle.

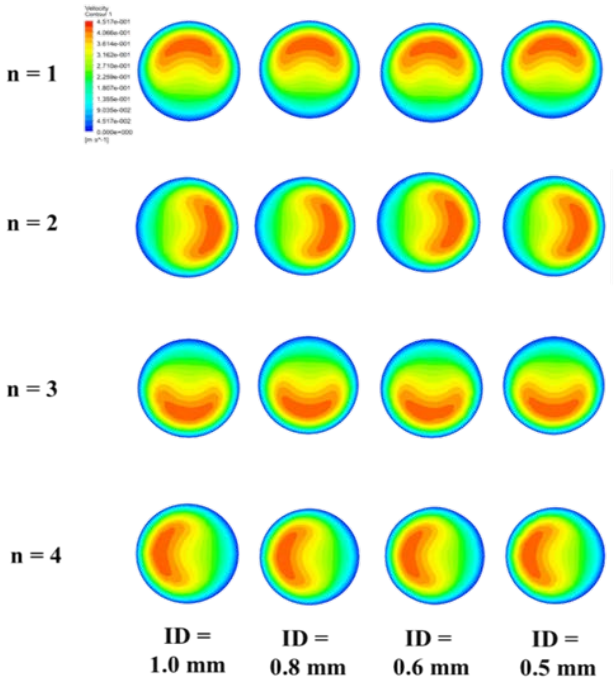

Fig 5. Velocity profile for MCFI constructed with tubing of 0.5≤ID≤1.0mm from the first arm (n=1) to the fourth arm (n=4)

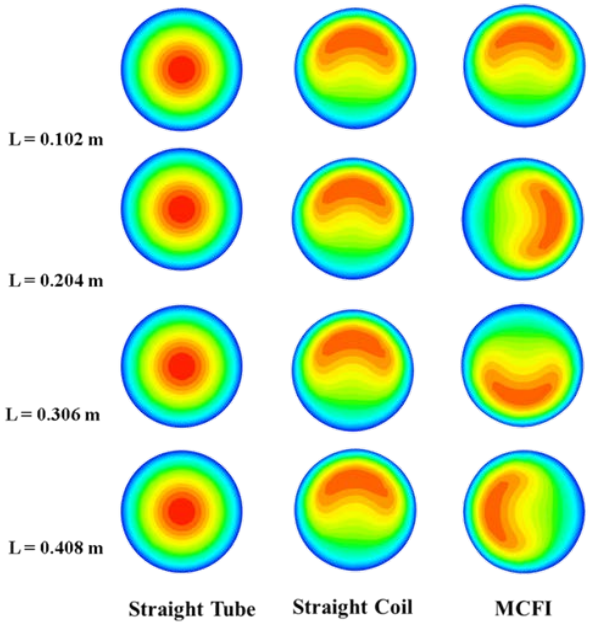

Fig 6 Velocity profile for different tubing configuration with 0.5mm ID with equal normalised tube length of L=0.102m

3.3 Mass Tranport

Simulation was initiated with a mass fraction of '1' for red dye at the top half of the inlet, and a mass fraction of '1' for blue dye at the bottom half. As the fluid progress within the MCFI, mixing occurred through both diffusion and flow inversion, causing the mass fraction value to decrease based on the extent of mixing. Mixing is considered ideal when a cell contained equal parts of both dyes, resulting in a local mass fraction of value of 0.5 for both species, represented by a bright green colour.

Cross sectional visualisation of fluid flow within the MCFI in Fig. 7 showed a secondary flow exerted on the fluid. Mass fraction contour suggested such that high velocity fluid moved from the centre of the tubing to the outer wall through the middle, while fluid at the outer wall moved along the upper and lower halves of the outer wall back to the inner wall. At the first arm (n=1), the fluid was showed to move from the bottom of the cross section (inner wall) to the top (outer wall). This created a circular turbulence flow within the MCFI even in laminar flow condition. After the fluid passed the 90˚ bend, this phenomenon rotated accordingly.As the region for maximum velocity was switched from side to side, the direction of secondary flow, in which fluid from high velocity region moved towards the outer wall, also rotated accordingly from left to right (n=2), top to bottom (n=3) and right to left (n=4).

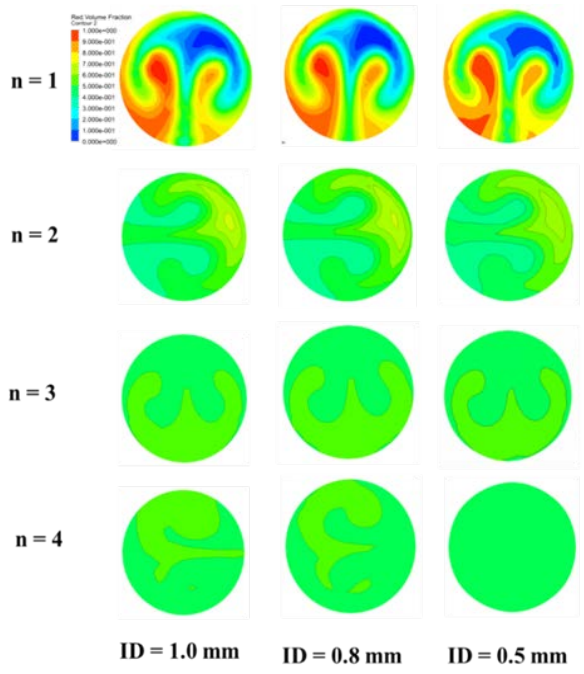

Fig. 7 Cross sectional mass fraction contour for MCFI from the first arm (n=1) to fourth arm (n=4)

From the mass fraction contour, it can be seen that the fluid in all the MCFI with tube diameter 1.0 mm, 0.8mm, 0.6mm and 0.5 mm had similar flow pattern and mixing profile. However, it was hard to discern the extend of mixing of MCFI based on the mass fraction contour alone, as only tubing with 0.5mm inner diameter showed complete mixing at the forth arm. Additional evaluation on the mixing profile of fluid in the MCFI was carried out by plotting the percentage of mixing over distance in travelled in tube length.

3.4 Mixing Plot

Fig. 8 shows the mixing plot for various tubing configurations investigated, in which the percentage of mixing is plotted against tube length to indicate the distance travelled by the liquids before complete mixing occurs. In order to fix the curvature ratio at 10, the total tube length used for the construction of the MCFI varied according to the tube diameter. To better visualise and compare the mixing rate of fluids in relation to the tube length, the graph was plotted with the normalised tube length with 1 representing the total tube length (L0) of each MCFI, and 0 representing the inlet.

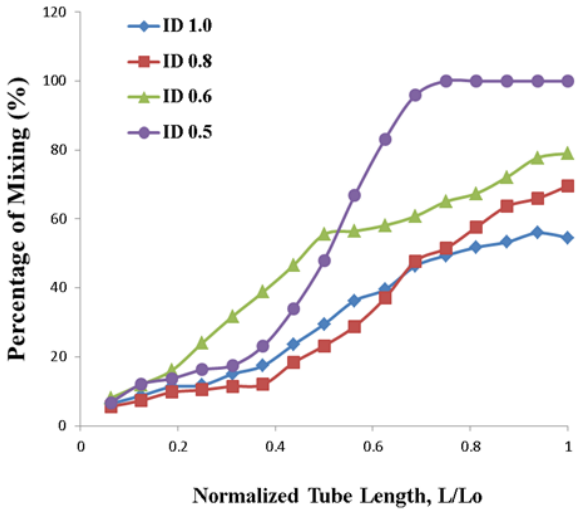

Fig. 8 Mixing plot for MCFI constructed with tubing of 0.5≤ID≤1.0mm

Mixing curves of the MCFI all portrayed shoulders with increased rate of mixing at approximately every five data point interval corresponding to the 90˚ bends of MCFI, though the extent of increment in mixing rate varied for different tube diameter. This observation supported that the presence of 90˚ bends improved the rate of mixing brought on by flow inversion.

MCFI with ID 1.0 mm showed the least rapid rate of mixing, and the increment brought on by flow inversion was least significant. The dyes exited the MCFI with 54.5% mixing. MCFI with ID 0.8 mm showed slightly improved mixing rate, whereby the increments after bending was slightly improved. However, the dyes still exited the MCFI with 69.6% mixing unable to achieve complete mixing. This condition was similar to tube with 0.6 mm diameter where fluid exited the MCFI with 78.9% mixing.

Referring to the plotted graph, it can be perceived that only MCFI with the tubing diameter of 0.5 mm achieved complete mixing, at 0.69 normalized tube length equivalent to 175mm. MCFI with ID 0.5 mm did not show the gradual increment in mixing rate caused by flow inversion as presented with larger-sized tubing. Instead, the mixing rate resembled a sigmoidal curve where it increased exponentially to achieve complete mixing before the fourth arm of the MCFI.

3.5 Comparison with Straight Tube and Straight Coil

As the MCFI with 0.5mm was able to achieve complete mixing, it was important to eliminate the possibility that the small cross sectional area had instead facilitated diffusive mixing, and that complete mixing was achieved simply by diffusion. Tubing configuration should be proved to have affected the mixing rate of the dyes. Hence, fluids were also made to interact in straight tube and straight coil similarly with 0.5 mm tube diameter.

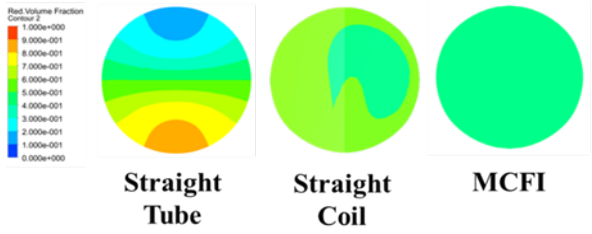

Fig. 8 Outlet cross-sectional mass fraction contour for straight tube, straight coil and MCFI

Upon investigation, dyes in straight tube and straight coil were unable to achieve complete mixing with tube length equivalent to the construction of MCFI. As shown in Fig. 9, the mass fraction contour at the outlet indicated that only MCFI achieved complete mixing when compared to straight tube and straight coil constructed with 0.5mm tubing. For the straight tube, the concentration gradient of both species was obvious with two layers which highlighted the molecular diffusion process. For straight coil, the mixing was improved significantly, although not complete.

Similarly, the percentage of mixing was plotted against normalized tube length for the different tubing configurations. Due to the high flow rate, the mixing rate in straight tube almost flat-lined where it exited the tube with only 7% mixing, while straight coiled did fared better with 54.6% mixing. This confirmed that the secondary flow in coiled configuration did improve the mixing compared to diffusive mixing, and in subsequence flow inversion improved secondary flow mixing.

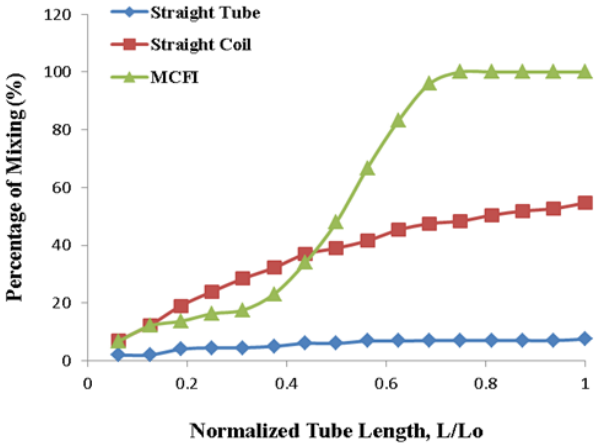

Fig.9 Comparison of MCFI mixing efficiency to straight tube and straight coil of 0.5 mm

4 Conclusion

This study presented the simulation of mixing profile of fluid within MCFI with varying tubing diameters of 1.0mm, 0.8mm, 0.6mm and 0.5mm. Besides the variance in tubing diameter, other parameters such as pitch and curvature ratio of the MCFI were identical to avoid complexity during the evaluation of mixing.

As anticipated, the reduction in tube diameter brought along an increase in pressure drop across the MCFI. Pressure drop plotted against tube diameter indicated an exponential increase in pressure with a corresponding reduction of tube diameter. Tubing with 1.0mm diameter showed the lowest pressure drop with 621 Pa, and the pressure increased in an almost exponential behaviour as the tube diameter was reduced gradually to 0.5mm reaching 24.95 kPa.

Secondary flow was observed in MCFI where fluid moved from the centre of the tubing to the

outer wall through the middle, while fluid at the outer wall moved along the upper and lower halves of the outer wall to the inner wall. Water-based dyes in the MCFI of different tubing diameter displayed negligible differences in flow pattern and mass transfer process as seen on the mass fraction contour.

Upon analysis of mixing plot, the effect of tubing diameter was established. Complete mixing was only achieved in MCFI with tube diameter of 0.5mm at normalized tube length of 0.69, equivalent to 175mm, before the fluid exited the MCFI. Larger tubing diameter led to incomplete mixing with 54.5% mixing (1.0 mm ID), 69.6% mixing (0.8 mm ID) and 78.9% mixing (0.6 mm ID) at the outlet, even though the fluid flow has the same Re of 250. Tubing configuration was proven to have affected the mixing rate of the dyes by comparing mixing in straight tube, straight coil and MCFI of similar tube diameter of 0.5 mm. Secondary flow in coiled configuration did improve the mixing compared to diffusive mixing, while flow inversion improved secondary flow mixing.

In conclusion, MCFI flow inversion improved the mixing condition in micro-structured tubing, in enhancement of the diffusive mixing in microfluidics. This may present MCFI as an alternative for microfluidic chip-based mixers, and find application in the constructions of microreactors. Though this finding might suggest that MCFI with smaller tubing diameter had more promising potential in mixing processes, further study can be carried out to verify this observation.

Acknowledgement

Both authors thank the support of Universiti Teknologi Malaysia in providing the facilities and software licensing for the implementation of this study.

References

[1] V. Kumar, M. Aggarwal, and K. D. P. Nigam. "Mixing in curved tubes." *Chemical Engineering Science*. 2006; 61(17): 5742-5753.

[2] M. Mridha, and K.D Nigam. "Coiled flow inverter as an inline mixer." *Chemical Engineering Science*. 2008 Mar; 63(6):1724-32.

[3] V. Kumar, M. Mridha, A.K. Gupta, and K. D. Nigam . "Coiled flow inverter as a heat exchanger." *Chemical Engineering Science*. 2007 May; 62(9):2386-96.

[4] V. Kumar, and K.D. Nigam "Numerical simulation of steady flow fields in coiled flow inverter". *International journal of heat and mass transfer*. 2005 Nov; 48(23):4811-28.

[5] M.M. Mandal, V. Kumar, and K. D. P. Nigam. "Augmentation of heat transfer performance in coiled flow inverter vis-à-vis conventional heat exchanger." *Chemical Engineering Science* 65, no. 2 (2010): 999-1007.

[6] M.M Mandal, P. Aggarwal, K.D. Nigam . "Liquid–liquid mixing in coiled flow inverter." *Industrial & Engineering Chemistry Research*. 2011 Jul; 50(23):13230-5.

[7] M.M. Mandal, C. Serra, Y. Hoarau, and K. D. P. Nigam. "Numerical modeling of polystyrene synthesis in coiled flow inverter." *Microfluidics and nanofluidics* 10, no. 2 (2011): 415-423.

[8] J. Singh, N. Kockmann, K.D. Nigam . "Novel three-dimensional microfluidic device for process intensification." *Chemical Engineering and Processing*: Process Intensification. 2014 Dec; 86:78-89.

[9] S.K. Kurt, M.G. Gelhausen, N. Kockmann. "Axial dispersion and heat transfer in a milli/microstructured coiled flow inverter for narrow residence time distribution at laminar flow." *Chemical Engineering & Technology*. 2015 Jul; 38(7):1122-30.

[10] S.K. Kurt, I.V Gürsel, V. Hessel, K.D. Nigam, and N. Kockmann. "Liquid–liquid extraction system with microstructured coiled flow inverter and other capillary setups for single-stage extraction applications." *Chemical Engineering Journal*. 2016 Jan 15; 284:764-77.

[11] L. Sharma, K. D. P. Nigam, and S. Roy. "Single phase mixing in coiled tubes and coiled flow inverters in different flow regimes." *Chemical Engineering Science*. 2017;160: 227-235.

[12] López-Guajardo, Enrique, et al. "Coiled flow inverter as a novel alternative for the intensification of a liquid-liquid reaction." *Chemical Engineering Science*. 2017, https://doi.org/10.1016/j.ces.2017.01.016.

[13] Gürsel, Iris Vural, S. K. Kurt, J. Aalders, Q. Wang, T. Noël, K. D. P. Nigam, N. Kockmann, and V. Hessel. "Utilization of milli-scale coiled flow inverter in combination with phase separator for continuous flow liquid–liquid extraction processes." *Chemical Engineering Journal* 283 (2016): 855-868.

[14] A.K. Sharma, H. Agarwal, M. Pathak, K. D.P. Nigam, and A. S. Rathore. "Continuous refolding of a biotech therapeutic in a novel

Coiled Flow Inverter Reactor." *Chemical Engineering Science* 140 (2016): 153-160.